ORIGINAL CONTRIBUTION

Tensile Behaviour of Corroded Strands in Prestressed Concrete Systems

Resmi Giriraju[1] · Amlan Kumar Sengupta[1] · Radhakrishna G. Pillai[1]

Abstract Corrosion of strands can cause brittle failure of prestressed concrete bridge girders. The present study experimentally investigated the effect of chloride-induced corrosion on the tensile behaviour of 7-wire strands commonly used in prestressed concrete structures. Five prism specimens with embedded strands were subjected to impressed current corrosion in chloride environment. The corroded strands were extracted, and their section loss profiles were obtained using Computed Tomography (CT) scanning technique. Pitting factor was used to quantify the severity of corrosion in a strand. The strand specimens were tested under tension to generate the average stress versus average strain curves for the corroded regions. It was found that the ductility of a strand was completely lost even at an average section loss of about 12%. Analytical models for the mechanical properties of the tensile behaviour of a corroded strand were developed. An attempt was made to estimate the pitting factor from the average section loss, that can be used for field applications in the absence of section loss profile for a corroded strand. Finally, the developed models were substantiated by comparing with the results of the tension tests. They were also corroborated using test results and theoretical predictions available in the literature.

Keywords Chloride-induced corrosion · Mechanical properties · Pitting factor · Prestressed concrete · Strand · Tensile behaviour

List of Symbols

$\Delta A_{avg,s}$	Average section loss of strand (%)
$\Delta A_{max,cw}$	Maximum section loss of critical wire (%)
$\Delta A_{max,s}$	Maximum section loss of strand (%)
$A_{res,s}$	Residual area of corroded strand (mm^2)
E_s	Modulus of elasticity of uncorroded strand (MPa)
E_{cs}	Modulus of elasticity of corroded strand (MPa)
f_p	Stress in strand (MPa)
f_{py}	Yield stress of uncorroded strand (MPa)
f_{py_cs}	Yield stress of corroded strand (MPa)
f_{pu}	Ultimate stress of uncorroded strand (MPa)
f_{pu_cs}	Ultimate stress of corroded strand (MPa)
k_E	Reduction factor for modulus of elasticity
k_{fpu}	Reduction factor for ultimate stress
$k_{\varepsilon u}$	Reduction factor for breaking strain
ℓ_c	Length of corroded region in the corroded strand (mm)
N_c	Number of corroded wires of a strand
N_{cc}	Number of critically corroded wires of a strand
P_f	Pitting factor
$P_{f,exp}$	Pitting factor obtained using data from CT scan images
$P_{f,model}$	Pitting factor obtained from analytical model
ε_p	Strain in strand
ε_y	Yield strain of uncorroded strand
ε_{y_cs}	Yield strain of corroded strand
ε_u	Breaking strain of uncorroded strand
ε_{u_cs}	Breaking strain of corroded strand

✉ Resmi Giriraju
  resmigiriraju2019@gmail.com

[1] Department of Civil Engineering, Indian Institute of Technology Madras, Chennai 600036, India

Introduction

Corrosion of the strands has led to many instances of premature failure in existing prestressed concrete (PC) bridge

868

J. Inst. Eng. India Ser. A (September 2022) 103(3):867–879

decks since 1980 [1–8]. The ingress of moisture and chloride ions occurring through either concrete cover (pre-tensioned girders) or end blocks (post-tensioned girders) is a primary reason for corrosion. For post-tensioned girders, it gets aggravated in case of improper grouting of the ducts [9]. The main difference between corrosion in a reinforced concrete member and that in a PC member is that less extent of pitting corrosion in the latter can trigger brittle failure of the component or the structure as a whole [10].

The quantitative evaluation of corrosion [11] can be broadly classified as non-localized average cross-section loss (gravimetric mass loss [12–15]) and localized maximum cross-section loss (pit-configurations [16–19], contour gauge [20, 21], three-dimensional geometric modelling using laser scanning [22]). Several studies showed that the tensile deformability and ductility of prestressing wires as well as strands are highly sensitive to corrosion. The post-yield branch of the stress versus strain curve even disappeared at a less extent of corrosion [14, 15, 17–19]. In case of a multi-wire strand, the corrosion level of the maximum (critically) corroded wire is significant to cause the failure of the strand [19]. This is the main reason for the less accurate predictions of the tensile stress versus strain behaviour of strands with average section loss less than 5% [18, 19]. Hence, a new method was introduced in the present study to consider the localized pitting of critically corroded wire, as well as the distribution of corrosion in the strand, for predicting the tensile behaviour of a strand.

The objective of the study was to develop a methodology to predict the tensile behaviour of corroded prestressing strands. The paper is organized in the following manner. First, the test specimen details, artificial corrosion technique and the tensile test set-up are discussed under the section materials and methods. This is followed by the results from experiments, development of analytical models and generation of synthetic stress–strain curves. Finally, the proposed model is corroborated using data from recent literature.

Materials and Methods

Specimen Design and Fabrication

Four uncorroded strand specimens and five corroded strand specimens (as obtained from concrete prisms) were used in this study. Prisms with cross-section of 100 mm × 100 mm and length of 750 mm, were selected to simulate corrosion of the strands while embedded in concrete. Each prism specimen was reinforced with one 12.7 mm nominal diameter low-relaxation strand [23] placed at the centre. The concrete mix proportion of coarse aggregate, fine aggregate, water and cement by weight was 2.94:1.96:0.36:1.0. The 7-day average cube compressive strength was 41.7 MPa. The coarse aggregate and fine aggregate used were granite of maximum size 20 mm and natural river sand, respectively. Ordinary Portland Cement of Grade 53 S [24] was selected.

Accelerated Corrosion of Strands

The impressed current technique was adopted to accelerate the diffusion of chloride ions through the concrete cover of a prism specimen. A small reservoir of plan inner dimension 200 mm × 45 mm was constructed at the middle of the top surface of a prism specimen, to contain 5% sodium chloride (NaCl) solution. The strand (anode) and the Nickel chromium mesh (cathode) were connected to the positive and negative terminals, respectively, of a direct current (DC) galvanostatic Regulated Power Supply (RPS) of 64 V as shown in Fig. 1. Multimeter was used to monitor the current passing through the circuit. The duration of current was monitored to attain a target amount of corrosion (mass loss) in the strand based on the Faraday's law (Table 1). Subsequently, the corroded strands were retrieved by breaking the prism specimens (P1 to P5), followed by cleaning procedure stipulated in ASTM G1-03 [11].

Tension Test of Strands

The uncorroded and corroded strand specimens of length 750 mm, were tested under tension to characterize the average stress versus average strain behaviour. The static tests were conducted based on the standard procedure of ASTM A1061/A1061M-2016 [25], at ambient temperature using a displacement-controlled test facility (Servo-hydraulic testing system MTS Model 311.32 of 1 MN capacity), as shown in Fig. 2. The stress can vary among the wires in a strand. Even within a wire, the stress can vary across the section due to the effect of residual stress [26]. Here, an average stress was considered across the section of a strand. The failure of a corroded strand is defined as the instant at which any one of the corroded wires ruptures [19]. Modified end grips were used for the strands to prevent localised failure at the end grip region. It consisted of hardened aluminium plates with smooth, semi-cylindrical grooves and coated with slurry (Grade 3-F aluminium oxide as abrasive and glycerine as carrier). In addition to this, aluminium foil was wrapped to protect the end portions of a strand specimen within the grip [19, 27].

The sudden rupture of corroded wires of a strand specimen would have damaged the external extensometers. Hence, the load and elongation were recorded using in-built load cell and extensometer of the testing machine. The extensometer recorded the total elongation between the grips. The slips occurring at the end grips were calibrated and deducted from the elongation, by conducting a parallel tension testing of an uncorroded strand specimen (Fig. 3).

J. Inst. Eng. India Ser. A (September 2022) 103(3):867–879

869

Fig. 1 Schematic diagram of artificial corrosion set-up
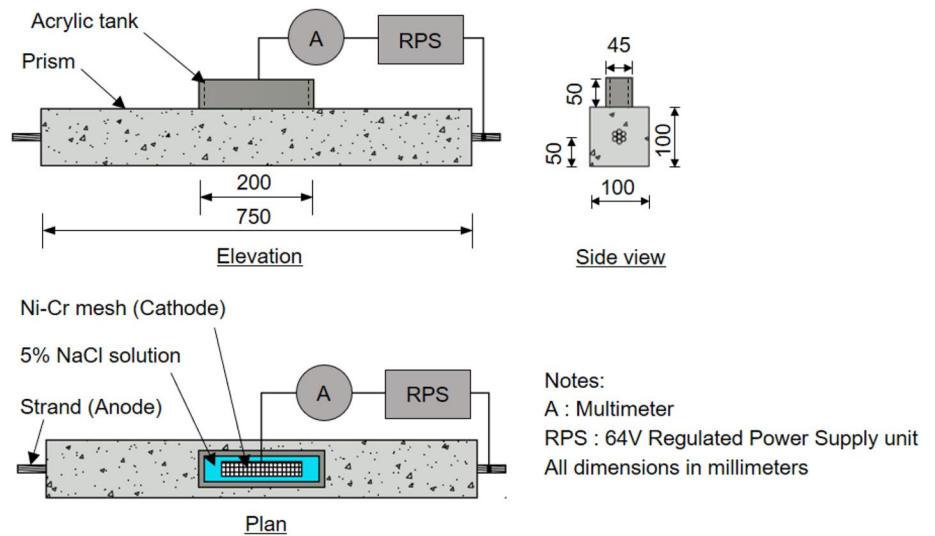
Table 1 Details of accelerated corrosion applied to prism specimens

Attributes	Units	P1	P2	P3	P4	P5
Exposure time	h	105.7	98.6	200.9	200.9	195.7
Intensity of current $\sum(I \times t)$	A-h	18.23	25.74	27.3	30.8	34.0
Current density	$\mu A/cm^2$	368.0	402.0	290.0	327.0	398.0
Target mass loss of strand	%	4.86	4.95	7.28	8.21	9.74
Actual mass loss	%	5.0	5.1	8.4	9.1	11.2
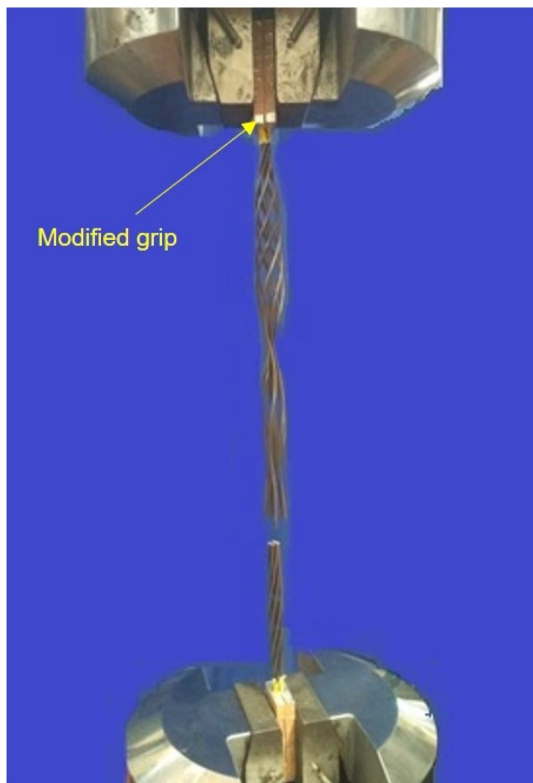
Fig. 2 Tension test set-up of a strand till failure

In the latter test, two LVDTs were fixed using magnetic base at the grip locations to obtain the slips till yielding of strand. It was assumed that additional slip after the yielding of a strand was negligible. The elongation between the grips was corrected by deducting the slips from the reading of the extensometer. An additional strain transducer was also attached at the middle region of the strand specimen to measure the strain in the test region. The strain calculated from the elongation was found to match with the strain obtained from the strain transducer. With this slip data as reference, slip excluded elongation was extracted for all the uncorroded and corroded strand specimens. For a corroded specimen, the net elongation of the corroded length was calculated by subtracting the elongations of the adjacent uncorroded lengths. The average strain in a corroded strand was calculated by dividing the net elongation by the measured length of the corroded region (ℓ_c). Here onwards, the average stress and average strain are simply referred to as stress and strain, respectively. The modulus of elasticity obtained in this paper is the apparent modulus of elasticity, as it is defined using average strain over a gage length.

870

J. Inst. Eng. India Ser. A (September 2022) 103(3):867–879
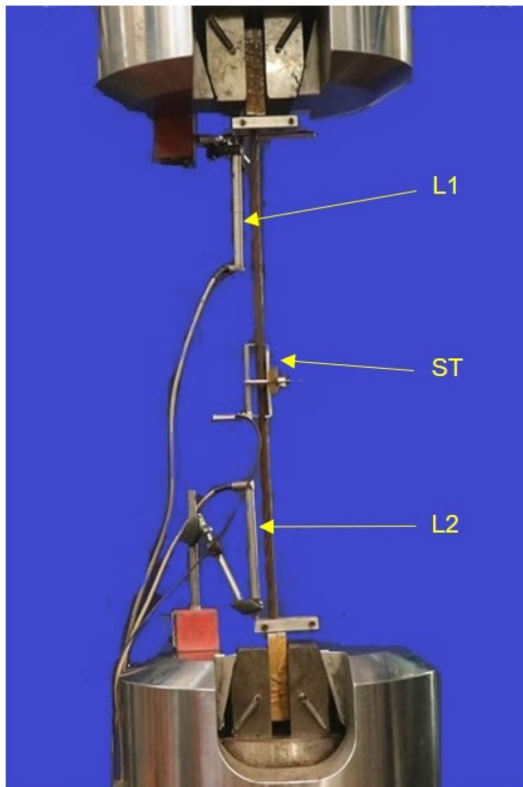
Note:
L1, L2 : LVDT of stroke length ±10 mm
ST : Strain Transducer of gage length 100 mm

Fig. 3 Tension test set-up of a strand till elastic limit to capture slip at end grips

Test Results and Analysis

Measure of Severity of Corrosion

The corrosion in strands was analysed after the tension tests of the specimens. The corrosion morphology of corroded strands showed severe pitting just beneath the reservoir region and slight pitting in the adjacent regions. The spatial distribution of section loss along the length of a strand was generated for all the corroded strands using X-ray Computed Tomography scanning technique (CT scan) (Table 2). This was done by analysing the transverse sectional images at every 1 mm interval along the length of a specimen. The length of a specimen had to be limited to 150 mm due to the space constraint of the scanning machine. The adopted technique was able to provide precise values of localised section loss along the length of a strand, as compared to the gravimetric method. It is evident from the corrosion morphology that with increasing corrosion, several uneven local pits (as in CS1 and CS2) get connected together to form a combination of smeared corrosion as well as pitting corrosion (as in

CS3, CS4 and CS5). This observation is in good agreement with the findings of Liu et al. [14].

In corrosion of metals, pitting factor (P_f) for a planar surface is used as a measure of severity of corrosion in terms of local pitting depth (P) and depth of uniform corrosion (d). It can be approximately defined as $P_f = P / d$. ASTM: G1-03 [11] also defines the pitting factor in a similar way. In the present study, for cylindrical surfaces of wires and strands, this concept was modified and defined as the ratio of maximum area loss of critical wire ($\Delta A_{max,cw}$) to average area loss of strand ($\Delta A_{avg,s}$) (Eq. (1) and Fig. 4). Thus, it considers both the maximum corrosion of the critically corroded wire, as well as the morphology of corrosion along the length of the strand. This concept is found to be similar to the cross-sectional area spatial heterogeneity factor defined by Zhang et al. [22]. Values of $\Delta A_{max,cw}$ and $\Delta A_{avg,s}$ could be extracted from the section loss profiles of the corroded strand specimens (Table 3). The value of P_f decreases with amount of corrosion, having a lower bound of approximately 1.0, as there will be more average area loss of the strand as compared to maximum area loss of the critical wire.

$$P_f = \frac{\Delta A_{max,cw}}{\Delta A_{avg,s}} \tag{1}$$

Analysis of Stress versus Strain Behaviour

The stress versus strain behaviour of uncorroded (US) strand of nominal diameter 12.7 mm was characterized for reference using four specimens (designated as US1 to US4). It was observed that the bi-linear stress–strain model
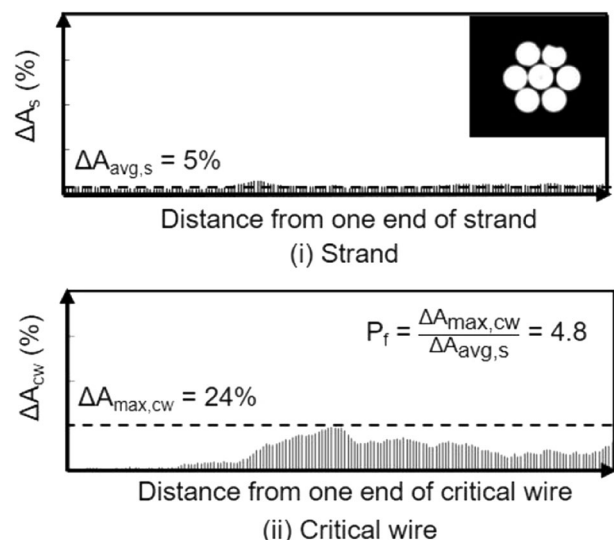

Fig. 4 Schematic representation of definition of pitting factor (P_f) of a corroded strand

is suitable for modelling the behaviour (Eq. (2)). This model can be conveniently modified to incorporate the effect of corrosion. The average mechanical properties of the uncorroded specimens are given in Table 4. As per IRC:112–2020 [28], the yield stress (f_{py}) was assumed to be $0.87f_{pu}$ and the corresponding yield strain as $\varepsilon_y = f_{py} / E_s$. The comparison of experimental results with the representative bi-linear model is shown in Fig. 5a.

For $\varepsilon_p \leq \varepsilon_y$,

$$f_p = \varepsilon_p E_s \tag{2a}$$

For $\varepsilon_y < \varepsilon_p \leq \varepsilon_u$,

Table 2 Maximum area loss of strand, section loss profile of critical wire (CW) and corrosion morphology of corroded strand
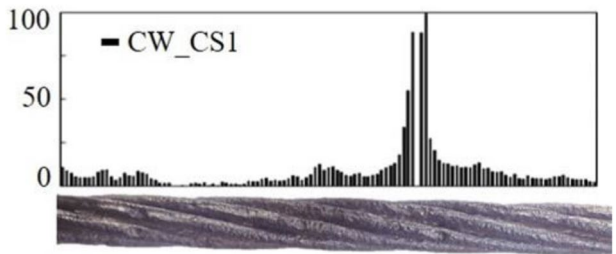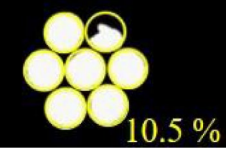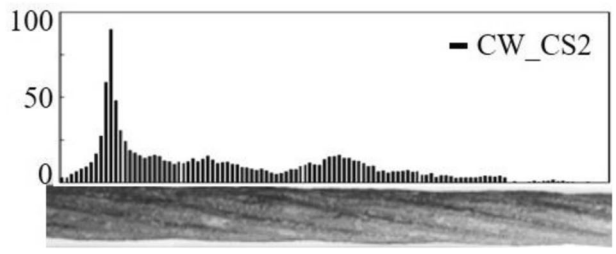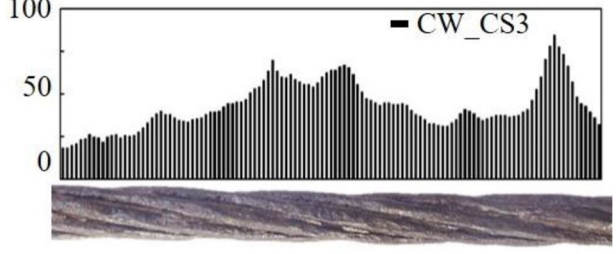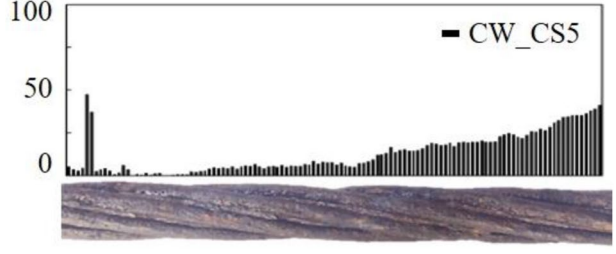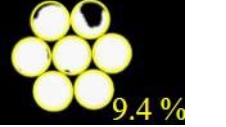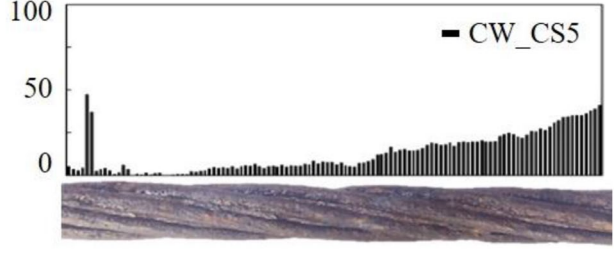
$\Delta A_{max,s}$ (%)	Section loss profile of critical wire and corrosion morphology
CS1 8.8 %	
CS2 10.5 %	
CS3 28.4 %	
CS4 26 %	
CS5 9.4 %	

872

J. Inst. Eng. India Ser. A (September 2022) 103(3):867–879

Table 3 Measured variables for obtaining pitting factor

Specimens	$\Delta A_{max,cw}$ (%)	$\Delta A_{avg,s}$ (%)	P_f
CS1	33.9	6.3	5.4
CS2	48.1	9.7	5.0
CS3	60.0	20.0	3.0
CS4	45.0	17.7	2.5
CS5	47.3	12.3	3.8

Table 4 Mechanical properties of uncorroded strand (US) specimens

Specimens	ε_u	f_{pu} (MPa)	E_s (MPa)
US1	0.082	1975.7	207,146
US2	0.052	1931.7	206,555
US3	0.073	1980.4	209,196
US4	0.066	1984.8	218,429
Average	0.068	1968.1	210,332

$$f_p = f_{py} + \frac{f_{pu} - f_{py}}{\varepsilon_u - \varepsilon_y} \times (\varepsilon_p - \varepsilon_y) \tag{2b}$$

In case of corroded strands, the elongation varied among the wires based on their residual areas. The average stress was calculated as the load divided by the average residual area of the corroded strand ($A_{res,s}$), which was obtained from $\Delta A_{avg,s}$. A sudden failure by rupture of the critically corroded wire was observed in all the specimens. Hence, the ultimate (breaking) load for a corroded strand was considered in this study to be governed by the critically corroded wire. ε_{u_cs}, f_{pu_cs}, E_{cs}, $A_{res,s}$ and ℓ_c are given in Table 5 for the

corroded strand specimens. Comparison of the average stress versus strain curves for corroded strands with the bi-linear model for uncorroded strand is shown in Fig. 5b. For higher level of corrosion ($\Delta A_{avg,s} > 12.3\%$), there was no yielding at all. The critical corrosion loss of 8% was considered to define no yield condition of corroded wires [14] and strands [18] in previous studies. Thus, the ductility of the strands was found to get reduced with increasing severity of corrosion. An analogous bi-linear stress–strain model is proposed for modelling the behaviour of a corroded strand using E_{cs}, ε_{y_cs}, and f_{py_cs} with (ε_{u_cs}, f_{pu_cs}) as the failure point (Eq. (3)). The yield stress (f_{py_cs}) is defined as $0.87f_{pu\_cs}$ for $f_{pu\_cs} \geq f_{py}$ and the corresponding yield strain as $\varepsilon_{y\_cs} = f_{py\_cs} / E_{cs}$. No yielding was observed for specimens with $f_{pu\_cs} < f_{py}$ (CS3, CS4 and CS5).

For $\varepsilon_p \leq \varepsilon_{y\_cs}$

$$f_{p\_cs} = \varepsilon_p E_{cs} \tag{3a}$$

For $\varepsilon_{y\_cs} < \varepsilon_p \leq \varepsilon_{u\_cs}$

$$f_{p\_cs} = f_{py\_cs} + \frac{f_{pu\_cs} - f_{py\_cs}}{\varepsilon_{u\_cs} - \varepsilon_{y\_cs}} \times (\varepsilon_p - \varepsilon_{y\_cs}) \tag{3b}$$

Development of Analytical Models

Models for Mechanical Properties

It was evident from the experimental results that the degradation of mechanical properties (E_{cs}, ε_{u_cs} and f_{pu_cs}) occur as a result of the corrosion of a strand. For a corroded strand with non-prismatic section, E_{cs} was calculated based on the
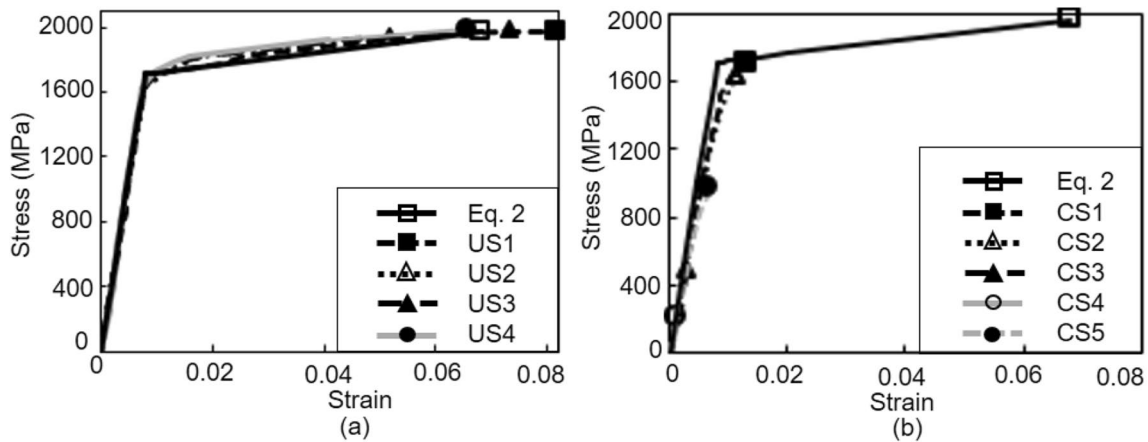
Note:
Eq. 2 – Representative bi-linear stress strain curve of uncorroded strand
All markers indicate the breaking point of critical wire of strand

Fig. 5 Average stress–strain curves (**a**) Uncorroded strands (US) (**b**) Corroded strands (CS)

Table 5 Measured variables of corroded strand (CS) specimens

Specimens	ε_{u_cs}	f_{pu_cs} (MPa)	E_{cs} (MPa)	$A_{res,s}$ (mm^2)	ℓ_c (mm)
CS1	0.0130	1710.4	193,813.9	92.5	365.0
CS2	0.0120	1631.3	187,310.7	89.1	400.0
CS3	0.0030	483.8	156,622.8	79.0	330.0
CS4	0.0014	202.6	145,925.3	81.2	385.0
CS5	0.0067	969.9	175,470.2	86.6	300.0

average behaviour over the corroded length. To consider the localized pitting of critically corroded wire as well as the distribution of corrosion in the strand, ε_{u_cs} and f_{pu_cs} were expressed in terms of P_f of the corroded strand. Each of these parameters were then normalised with respect to their corresponding values in uncorroded condition to get the reduction factors k_E, $k_{\varepsilon u}$ and k_{fpu} as shown in Eqs. (4), (5) and (6).

$$k_E = \frac{E_{cs}}{E_s} \tag{4}$$

$$k_{\varepsilon u} = \frac{\varepsilon_{u\_cs}}{\varepsilon_u} \tag{5}$$

$$k_{fpu} = \frac{f_{pu\_cs}}{f_{pu}} \tag{6}$$

The analytical models developed using experimental data points are shown in Fig. 6. They are expressed as follows.

$$k_E = a\Delta A_{avg,s} + b \tag{7}$$

$$k_{\varepsilon u} = c e^{f P_f} + g \tag{8}$$

$$k_{fpu} = h\, e^{m\, P_f} + n \tag{9}$$

The coefficients of Eqs. (7), (8) and (9) were derived from regression analysis and were obtained as: a = − 0.019, b = 1.0; c = − 1.306, f = − 0.092, g = 1.048; h = − 4.800, m = − 0.660 and n = 1.0. These models satisfied the bounding limits. The upper and lower limits used in each model are as follows. (i) $k_E = 1$ for $\Delta A_{avg,s} = 0\%$ and $k_E = 0$ for for
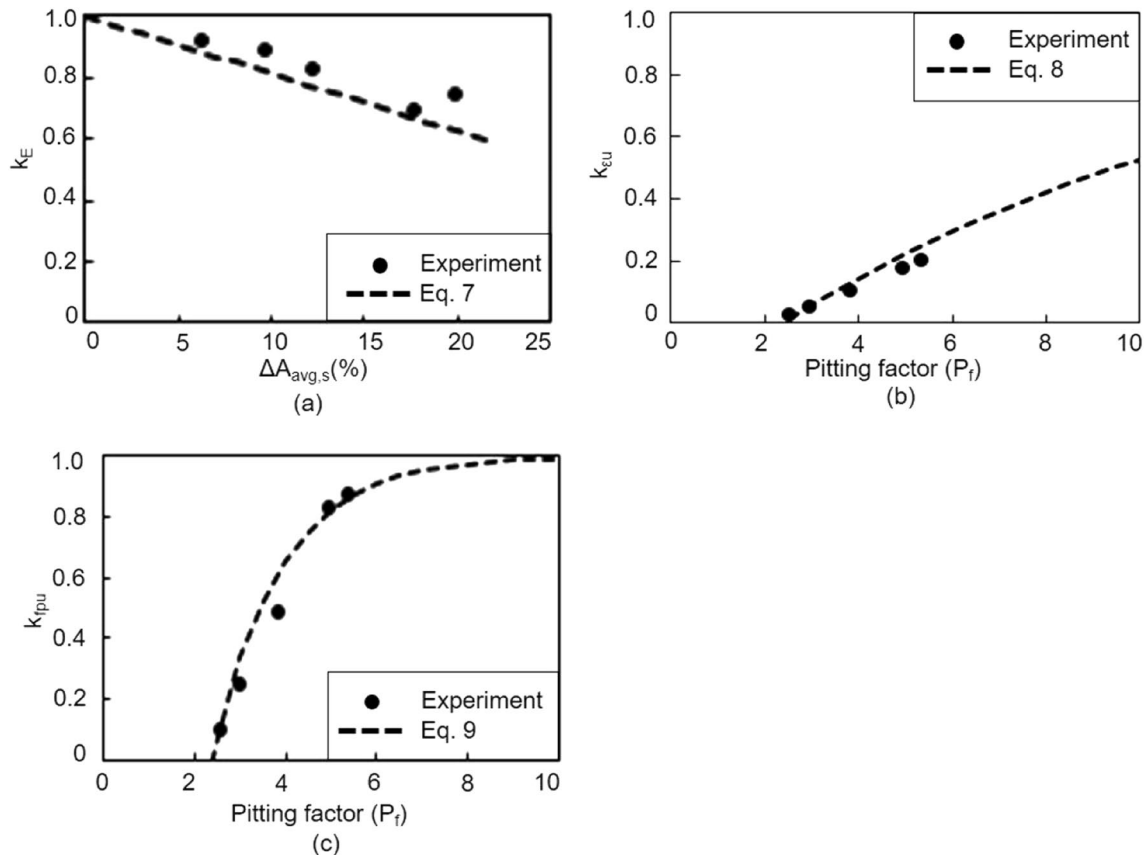

Fig. 6 Analytical models (**a**) k_E versus average section loss of strand (**b**) $k_{\varepsilon u}$ versus pitting factor and (**c**) k_{fpu} versus pitting factor

$\Delta A_{avg,s} = 53\%$ (ii) $k_{\varepsilon u} = 1$ for $P_f \geq 40$ and $k_{\varepsilon u} = 0$ for $P_f \leq 2.3$ (iii) $k_{fpu} = 1.0$ for $P_f \geq 40$ and $k_{fpu} = 0$ for $P_f \leq 2.3$.

Pitting Factor for a Corroded Strand

In absence of CT scan results, to get P_f of a corroded strand specimen, it needs to be related to the commonly computed data $\Delta A_{avg,s}$. It was observed that at a section, the residual areas of the individual wires can be different in strands with same $\Delta A_{avg,s}$ [29]. Hence, the number of severely corroded wires (N_{cc}) and corroded wires (N_c) were both incorporated in relating the pitting factor for a given $\Delta A_{avg,s}$. The value of N_{cc} can be more than 1, based on the method of corrosion. The model relating P_f and $\Delta A_{avg,s}$ (Eq. (10)) was developed based on N_{cc} and N_c data of the experimental corroded strand specimens (Table 6). P_f gets reduced if both N_{cc} and N_c are more for a given $\Delta A_{avg,s}$. The comparison of P_f obtained from proposed model and that from experiments is given in Fig. 7.

$$P_f = \frac{5}{N_{cc}N_c}\left(\frac{p}{\Delta A_{avg,s}} + q\right) \tag{10}$$

The coefficients of Eq. 10 were derived from regression analysis and were obtained as: $p = 37.6$ and $q = 0.69$.

In an existing bridge girder, the rate of corrosion of strand (mm/year) can be obtained from the instrument such as GECOR-9, which works based on linear polarization resistance (LPR) technique. The $\Delta A_{avg,s}$ can be estimated from this data by adopting an appropriate area loss model for a corroding strand. N_c and N_{cc} can be obtained based on the diffusion of chloride front through the concrete cover and wire orientation of strand. Hence, P_f can be estimated using Eq. 10. The $\Delta A_{avg,s}$ and P_f can be used for further analysis of existing girder. Thus, P_f can be used in field to get the severity of pitting corrosion of critical wire of each strand in existing structures from the measured rate of corrosion data.
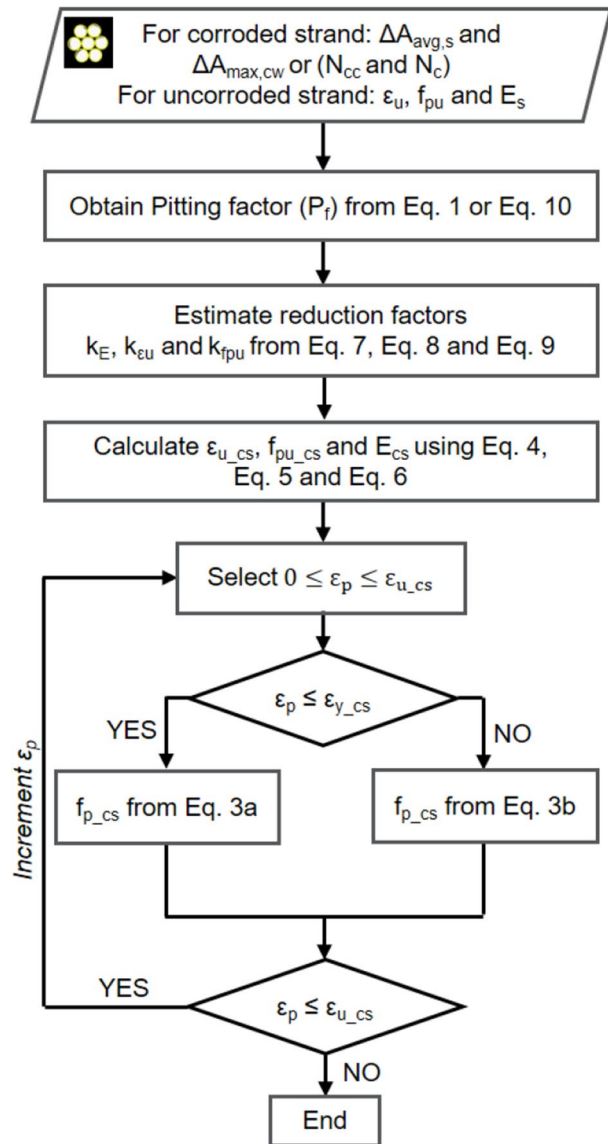
Table 6 Values of N_{cc} and N_c for corroded strands

Variables	CS1	CS2	CS3	CS4	CS5
N_{cc}	1	1	1	1	1
N_c	6	5	6	5	5
$P_{f,model}$	5.6	4.6	2.6	2.8	3.1
$P_{f,exp}$	5.4	5.0	3.0	2.5	3.8
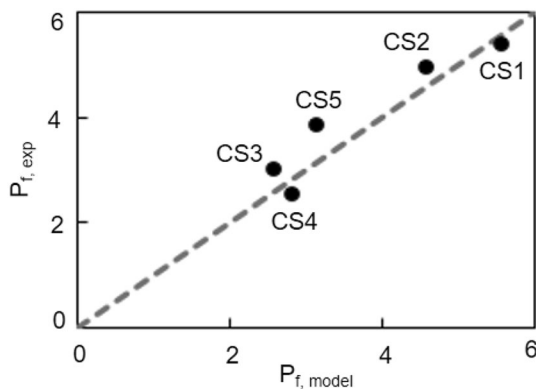
Fig. 7 Comparison of pitting factor obtained from proposed model and experiment

Fig. 8 Flowchart for theoretical prediction of average stress versus strain curves of corroded strand
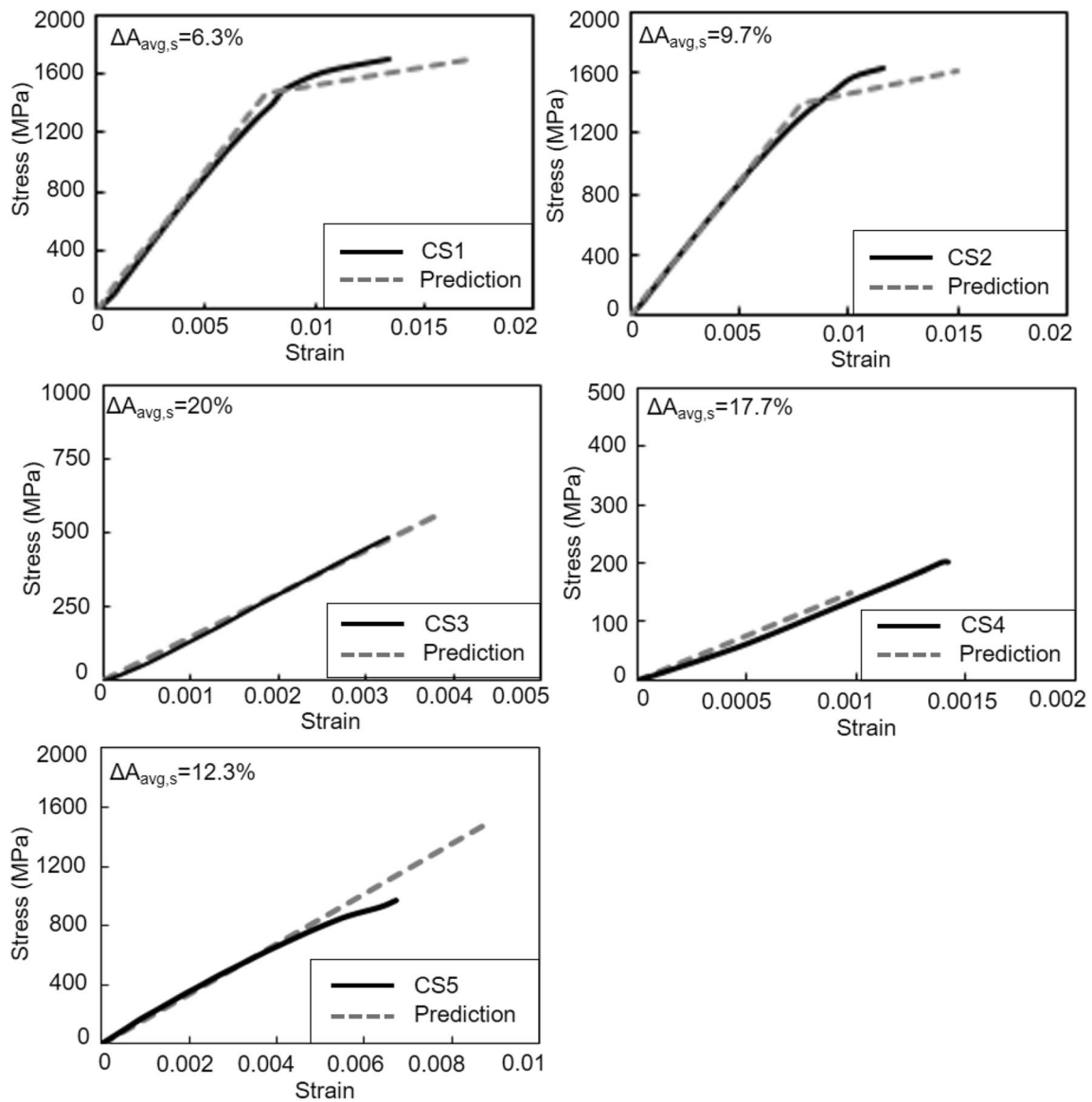
Fig. 9 Comparison of experimental data and theoretical prediction of average stress versus strain behaviour of corroded strands

Prediction of Stress Versus Strain Curves

The methodology adopted for developing the stress versus strain curve of any corroded strand is given in Fig. 8 as a flowchart. The results obtained from the tensile tests of the corroded strands were then compared with the corresponding predicted stress–strain curves, as shown in Fig. 9. Here, the pitting factor obtained from section loss profile was used. It was found that the theoretical prediction of stress–strain curve is in reasonable agreement with the tensile test results. The loss of ductility can be modelled by limiting the capacity of the strand corresponding to the breaking strain. Minor deviations of the predicted curves from the experimental results are due to the irregularity and variability of pitting corrosion along the lengths of the strands.
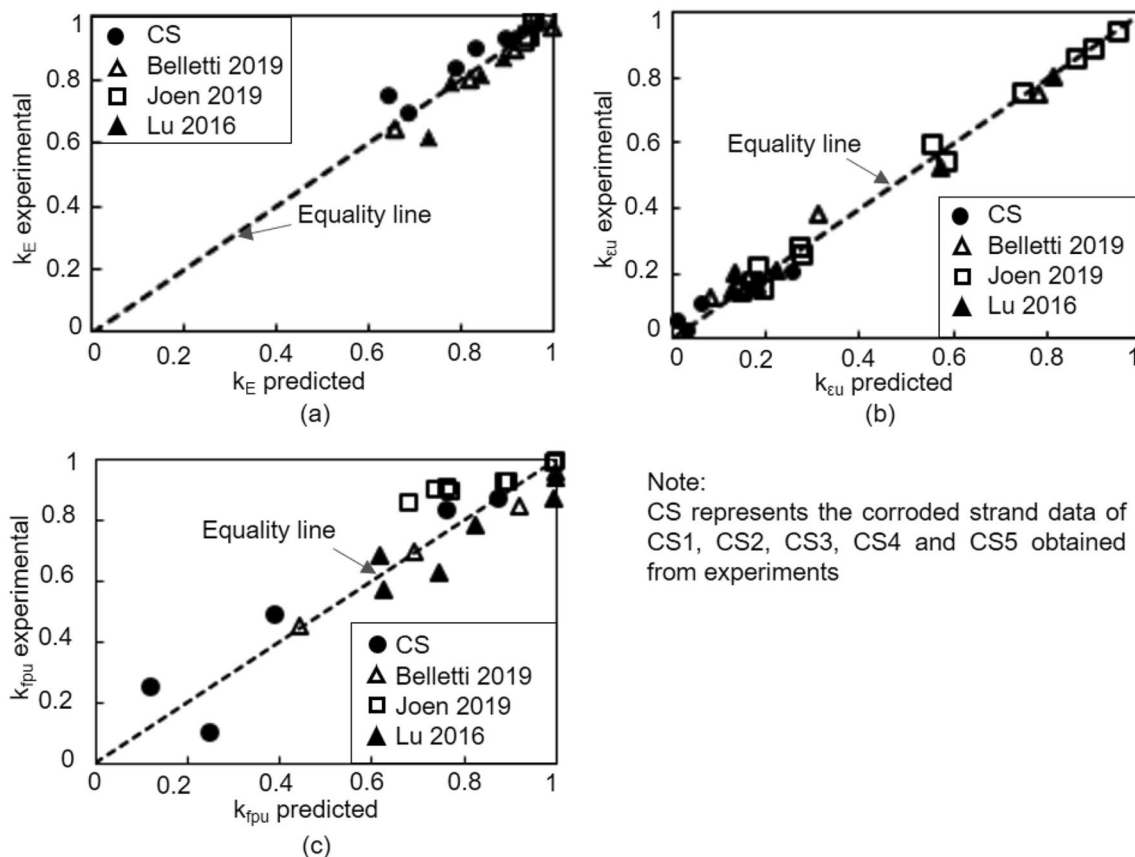
Fig. 10 Comparisons of proposed models for reduction factors with available experimental data (**a**) Modulus of elasticity, k_E, (**b**) Breaking strain, $k_{\varepsilon u}$, (**c**) Ultimate stress, k_{fpu}

Validation of Developed Models

The developed models were used to corroborate the parameters for corroded strands with the data obtained from the test results in the available literature [15, 18, 19]. Values of $\Delta A_{avg,s}$ were available for the specimens of Jeon et al. [19] and Belletti et al. [15], which were naturally corroded strands from existing structures. Values of $\Delta A_{max,s}$ obtained from the specimens of Lu et al. [18] were converted to $\Delta A_{avg,s}$ using a relationship established from experiments. In the absence of details about the number of corroded wires which contributed to $\Delta A_{avg,s}$, N_{cc} and N_c were evaluated based on the best fit with the corresponding experimental data. The plots for correlation of theoretical and experimental values of reduction factors k_E, $k_{\varepsilon u}$ and k_{fpu} are shown in Fig. 10, having coefficients of correlation equal to 0.89, 0.99 and 0.87, respectively. Additionally, the accuracy of proposed method was checked and compared with the available theoretical predictions of Jeon et al. [19] and Lu et al. [18], as shown in Fig. 11. The available section loss models

for pitting corrosion such as Type 1, Type 2 and Type 3 pit configurations were used in Jeon et al. [19], whereas a hemispherical pit model was adopted in Lu et al. [18]. It can be seen that the proposed models are giving reasonably good predictions for k_E and $k_{\varepsilon u}$ when compared to the experimental data. Further studies are required to refine the proposed model for better prediction of k_{fpu}.

Influence of Steel Micro-Cracking

The development of steel micro-cracking emanating from the pits can be attributed to the presence of synergic effects of stress, corrosive medium, diffusion of corrosive hydrogen and material properties. Figure 12 shows the presence of micro-cracks in one of the corroded strand specimens captured using Scanning Electron Microscopy (SEM). The local effects caused by such damage would have led to the reduction of apparent elastic modulus and brittle failure [30]. The degradation due to corrosion in existing PC bridge girders can be similar to that discussed above.
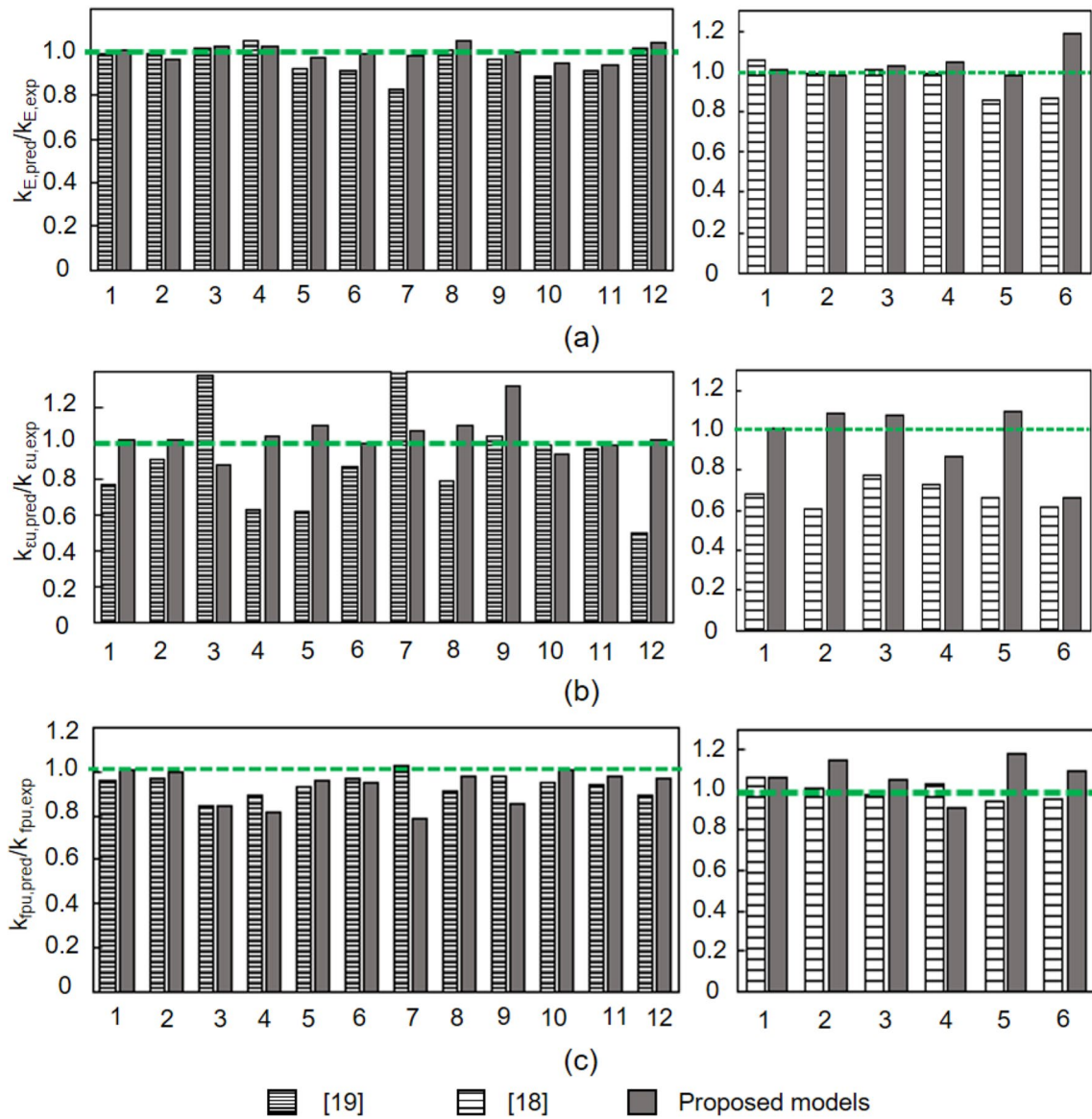
J. Inst. Eng. India Ser. A (September 2022) 103(3):867–879

877

Fig. 11 Comparison of proposed models for reduction factors with available theoretical predictions (**a**) $k_{E,pred}/k_{E,exp}$ (**b**) $k_{\varepsilon u,pred}/k_{\varepsilon u,exp}$ (**c**) $k_{fpu,pred}/k_{fpu,exp}$

878

J. Inst. Eng. India Ser. A (September 2022) 103(3):867–879
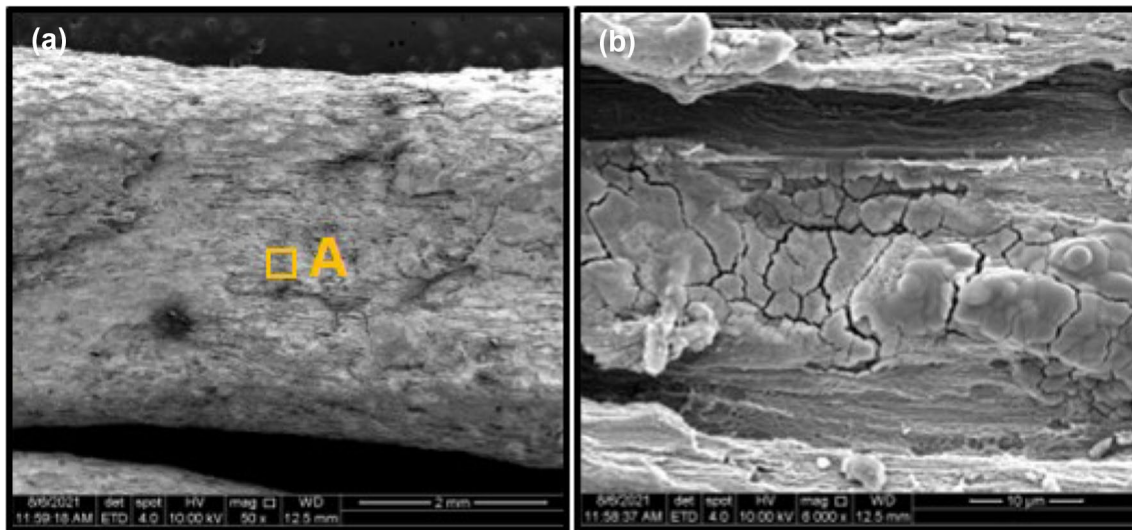
Fig. 12 Scanning electron microscope image of the pit region of a corroded wire of strand (**a**) 100μm magnification (**b**) Micro-cracks of Region A at 20μm magnification

Conclusions

This study primarily investigated the effect of sectional area loss on average tensile stress versus strain behaviour of corroded 12.7 mm diameter 7-wire strands. The major conclusions of the present study are as follows:

1) The level of corrosion of a single wire with respect to the average corrosion of the wires is significant to cause the failure of the strand. This aspect is considered in the proposed analytical models.
2) The severity of corrosion in a strand was defined in terms of the pitting factor (Eq. (1)). The values of the factor for the corroded strand specimens were obtained from the CT scan results. The values become smaller as the corrosion increases. Analytical models were developed to predict the pitting factor from an estimable quantity, such as the average section loss of the strand ($\Delta A_{avg,s}$, Eq. (10)).
3) The three mechanical properties of the tensile behaviour of a corroded strand, modulus of elasticity (E_{cs}), ultimate strength (f_{pu_cs}), and breaking strain (ε_{u_cs}), were obtained from tensile tests. It was observed that with increasing corrosion, the ductility of the strands gets reduced significantly. For $\Delta A_{avg,s} > 12.3\%$, there was no yielding in the average stress versus strain curve of a strand. Models were developed for predicting the reductions of E_{cs}, ε_{u_cs} and f_{pu_cs} (Eqs. (7), (8) and (9)).
4) The developed models in this study were substantiated by comparing with the results of the tension tests. They were also corroborated using test results and theoretical predictions available in the literature.

More number of corroded samples can be used to generate a database for refining the analytical models developed in this study. The study can be extended to corroded strand specimens subjected to prestress and fatigue loading behaviour.

Declarations

References

1. M. Schupack, M.G. Suarez, "Some recent corrosion embrittlement failures of prestressing systems in the United States. PCI J **27**(2), 38–55 (1982)

J. Inst. Eng. India Ser. A (September 2022) 103(3):867–879

879

2. N. Vladimir, Prestressed bridges and marine environment. J. Struct. Eng. ASCE **116**(11), 3191–3205 (1990). https://doi.org/10.1061/(ASCE)0733-9445(1990)116:11(3191)

3. R.J. Woodward, D.L.S. Wilson, Deformation of segmental post-tensioned precast bridges as a result of corrosion of the tendons. Proceed Institut Civil Eng (London) Part 1–Design Constr (1991). https://doi.org/10.1680/iicep.1991.14036

4. W. Podolny, Corrosion of prestressing steels and its mitigation. PCI J (1992). https://doi.org/10.15554/pcij.09011992.34.55

5. C. Sly, An initial look at the Lowe's motor speedway pedestrian bridge collapse. J. Fail. Anal. Prev. **1**(2), 7–9 (2001). https://doi.org/10.1007/BF02715154

6. A. Valiente, Stress corrosion failure of large diameter pressure pipelines of prestressed concrete. Eng Fail Anal **8**(3), 245–261 (2001). https://doi.org/10.1016/S1350-6307(00)00010-8

7. D. Trejo, M. B. D. Hueste, P. Gardoni, R. G. Pillai, K. Reinschmidt, S.B. Im, S. Kataria, S. Hurlebaus, M. Gamble, T T. Ngo, "Effect of voids in grouted post-tesioned concrete bridge construction: electrochemical testing and reliability assessment." *Austin: Texas Transportation Institute*, FHWA/TX-09/0–4588–1 Vol. 1, http://tti.tamu.edu/documents/0-4588-1-Vol1.pdf (2009)

8. R.A. Rogers, L. Wotherspoon, A. Scott, J.M. Ingham, Residual strength assessment and destructive testing of decommissioned concrete bridge beams with corroded pretensioned reinforcement. PCI J (2012). https://doi.org/10.15554/pcij.06012012.100.118

9. R.G. Pillai, M.D. Hueste, P. Gardoni, D. Trejo, K.F. Reinschmidt, Time-variant service reliability of post-tensioned, segmental, concrete bridges exposed to corrosive environments. Eng Struct **32**, 2596–2605 (2010). https://doi.org/10.1016/j.engstruct.2010.04.032

10. ACI 222.2R-01, Corrosion of Prestressing Steels, American Concrete Institute (2001)

11. ASTM: G1–03, Standard Practice for Preparing, Cleaning, and Evaluation *Corrosion Test Specimens*, ASTM International (2003)

12. L. Dai, L. Wang, J. Zhang, X. Zhang, A global model for corrosion-induced cracking in prestressed concrete structures. Eng Fail Anal **62**, 263–275 (2016). https://doi.org/10.1016/j.engfailanal.2016.01.013

13. W. Zhang, X. Liu, X. Gu, Fatigue behavior of corroded prestressed concrete beams. Constr Build Mater **106**, 198–208 (2016). https://doi.org/10.1016/j.conbuildmat.2015.12.119

14. X. Liu, W. Zhang, X. Gu, Y. Zeng, Degradation of mechanical behavior of corroded prestressing wires subjected to high-cycle fatigue loading. J Bridge Eng, ASCE **22**(5), 1–13 (2017). https://doi.org/10.1061/(ASCE)BE.1943-5592.0001030

15. B. Belletti, F. Vecchi, C. Bandini, C. Andrade, J.S. Montero, Numerical evaluation of the corrosion effects in prestressed concrete beams without shear reinforcement. Struct Concr **21**(5), 1794–1809 (2020)

16. M.G. Stewart, Spatial variability of pitting corrosion and its influence on structural fragility and reliability of RC beams in flexure. Struct Saf **26**(4), 453–470 (2004). https://doi.org/10.1016/j.strusafe.2004.03.002

17. M.S. Darmawan, M.G. Stewart, Effect of pitting corrosion on capacity of prestressing wires. Magaz Concr Resear **59**(2), 131–139 (2007). https://doi.org/10.1680/macr.2007.59.2.131

18. Z.-H. Lu, F. Li, Y.-G. Zhao, "An investigation of degradation of mechanical behaviour of prestressing strands subjected to chloride attacking." Proceedings of 5th International Conference on Durability of Concrete Structures. 57–65, DOI: https://doi.org/10.5703/1288284316111 (2016)

19. C.H. Jeon, J.B. Lee, S. Lon, C.S. Shim, Equivalent material model of corroded prestressing steel strand. J. Mater. Res. Tech. **8**(2), 2450–2460 (2019). https://doi.org/10.1016/j.jmrt.2019.02.010

20. L. Wang, X. Zhang, J. Zhang, Y. Ma, Y. Xiang, Y. Liu, Effect of insufficient grouting and strand corrosion on flexural behavior of PC beams. Constr Build Mater **53**, 213–224 (2014). https://doi.org/10.1016/j.conbuildmat.2013.11.069

21. X. Zhang, L. Wang, J. Zhang, Y. Ma, Y. Liu, Flexural behavior of bonded post-tensioned concrete beams under strand corrosion. Nucl Eng Design **313**, 414–424 (2017). https://doi.org/10.1016/j.nucengdes.2017.01.004

22. W. Zhang, B. Zhou, X. Gu, H. Dai, Probability distribution model for cross-sectional area of corroded reinforcing steel bars. J. Mater. Civ. Eng. **26**(5), 822–832 (2013). https://doi.org/10.1061/(ASCE)MT.1943-5533.0000888

23. IS 14268:2017, Uncoated stress relieved low relaxation seven-wire (Ply) *strand for Prestressed Concrete— Specification (First Revision)*, Bureau of Indian Standards (2017)

24. IS 12269:2013, Indian Standard Ordinary Portland Cement, 53 Grade — Specification., Bureau of Indian Standards (2013)

25. ASTM: A1061/A1061M, Standard Test Methods for Testing Multi-Wire Steel *Prestressing Strand,* ASTM International (2016)

26. J.M. Atienza, J. Ruiz-Hervias, M. Elices, The role of residual stresses in the performance and durability of prestressing steel wires. Exp. Mech. **52**(7), 881–893 (2012). https://doi.org/10.1007/s11340-012-9597-1

27. J.K. Kim, J.S. Kim, S.H. Kwon, Mechanical properties of a new prestressing strand with ultimate strength of 2160 MPa. KSCE J Civil Eng **18**(2), 607–615 (2014). https://doi.org/10.1007/s12205-014-0065-6

28. IRC: 112–2020, Code of practice for concrete road bridges, The Indian Road Congress (2020)

29. C.H. Jeon, C.D. Nguyen, C.S. Shim, Assessment of mechanical properties of corroded prestressing strands. Appl Sci (2020). https://doi.org/10.3390/app10124055

30. N.A. Vu, A. Castel, R. François, Effect of stress corrosion cracking on stress-strain response of steel wires used in prestressed concrete beams. Corros Sci **51**(6), 1453–1459 (2009). https://doi.org/10.1016/j.corsci.2009.03.033